CARAMEL: Contamination And Reliability Analysis of MicroElectromechanical Layout

Abhijeet Kolpekwar, Tao Jiang, and R. D. (Shawn) Blanton

Abstract—**CARAMEL (Contamination And Reliability Analysis of MicroElectromechanical Layout) is a CAD tool for MEMS fault model generation. It is based on the integrated circuit contamination analysis tool CODEF [1] and is capable of analyzing the impact of contamination particles on the behavior of microelectromechanical systems. CARAMEL's simulation output indicates that a wide range of defective structures are possible due to the presence of particulate contaminations. Moreover, electromechanical simulations of CARAMEL's mesh representations of defective layout has revealed that a wide variety of misbehaviors are associated with these defects. Several thousand contamination simulations were performed using CARAMEL on the surface micromachined comb-drive resonator. The results generated by CARAMEL identifies the comb drive as the most defect prone region of the microresonator and the deposition of the first structural layer as the most vulnerable processing step. [383]**

Index Terms—**Defects, faults, MEMS tests, resonator.**

I. Introduction

THE development and deployment of new MEMS products will not occur due to advances in design, packaging and processing alone. Testing methodologies must be developed in concert that are capable of assessing faulty behavior (in the form of fault simulation and automatic test pattern generation) along with design for testability (DFT) structures that improve and ensure the end quality of MEMS-based products. It should also be noted that many new and existing MEMS applications are integral parts of safety-critical systems. Consequently, the need to address reliability of MEMS makes the testability problem that much more important. To ensure high quality and reliability of MEMS, a comprehensive testing methodology must be developed that allows devices to be tested economically with a very high level of confidence. Success of any testing methodology is highly dependent on the fault models employed. Fault models that do not "cover" real defective behavior can reduce defect coverage and degrade test quality. The work presented here addresses this need.

MEMS fault models, unlike their digital and analog counterparts, must explicitly consider the impact of defects on the micromechanical structures. Our first step toward developing effective MEMS fault models centers on the inductive generation of faulty behaviors from particle contamination simulations. We have chosen the folded-flexure comb-drive microresonator[1] as our research vehicle because it possesses many of the basic structures (beams, joints, springs, etc.) that can form the core primitives of a MEMS design library [2]–[4]. We believe this analysis of the resonator will provide the basis for developing generic fault models that are applicable to a wide class of surface-micromachined MEMS.

MEMS failures can result from stiction, manufacturing variations, undesired residual stress, and particulate contaminations. Our experience is that a major cause of the hard-to-detect faulty behavior in MEMS is due to particulate contaminations that occur during and after various process steps of fabrication [5]. Particulates can cause a significant perturbation in the structural and material properties of the microstructure [6]. Thus, a formal assessment of both the possible defective structures and the corresponding faulty behaviors of MEMS design primitives will lead to the formation of effective MEMS fault models. Such fault models will undoubtedly lead to methods for fault grading, test generation, design-for-testability, and design for fault avoidance. The fault modeling process can also be used to form links between defects and faulty behaviors. Such links would aid in diagnosis by helping identify the process steps that are likely to produce the observed faulty behavior [7].

We have enhanced the process simulator CODEF [1] into a tool called CARAMEL (Contamination And Reliability Analysis of MicroElectromechanical Layout) for analyzing the impact of contamination particulates on the properties of microelectromechanical structures. CARAMEL is an integral component of our MEMS fault model generation (see Fig. 1). CARAMEL performs process simulation and creates a three-dimensional (3-D) representation of the defective microelectromechanical structure. It then extracts a mesh netlist representation from the defective structure whose form is completely compatible with the mechanical simulator ABAQUS [8]. Mechanical simulation of the mesh then allows us to link the contamination of concern to a defective structure and a faulty behavior. Observed faulty behaviors are then classified and used to form fault models at the next level of abstraction. Monte Carlo iteration around the flow of Fig. 1 provides a mechanism for creating realistic fault models for MEMS.

Here, we describe CARAMEL and illustrate its use in MEMS fault model generation. The resonator structure (see

Manuscript received August 31, 1998; revised March 19, 1999 and June 25, 1999. This work was supported by the National Science Foundation under Grant MIP-9702678 and the Defense Research Projects Agency under Rome Laboratory, Air Force Materiel Command, USAF, under Grant F30602-97-2-0323. Subject Editor, W. N. Sharpe, Jr.

The authors are with the Electrical and Computer Engineering Department, Center for Electronic Design Automation, Carnegie Mellon University, Pittsburgh, PA 15213-3890 USA.

Publisher Item Identifier S 1057-7157(99)07194-2.

[1] In the remaining parts of this paper, we will refer to the folded-flexure comb-drive microresonator simply as the "resonator."

1057–7157/99$10.00 © 1999 IEEE

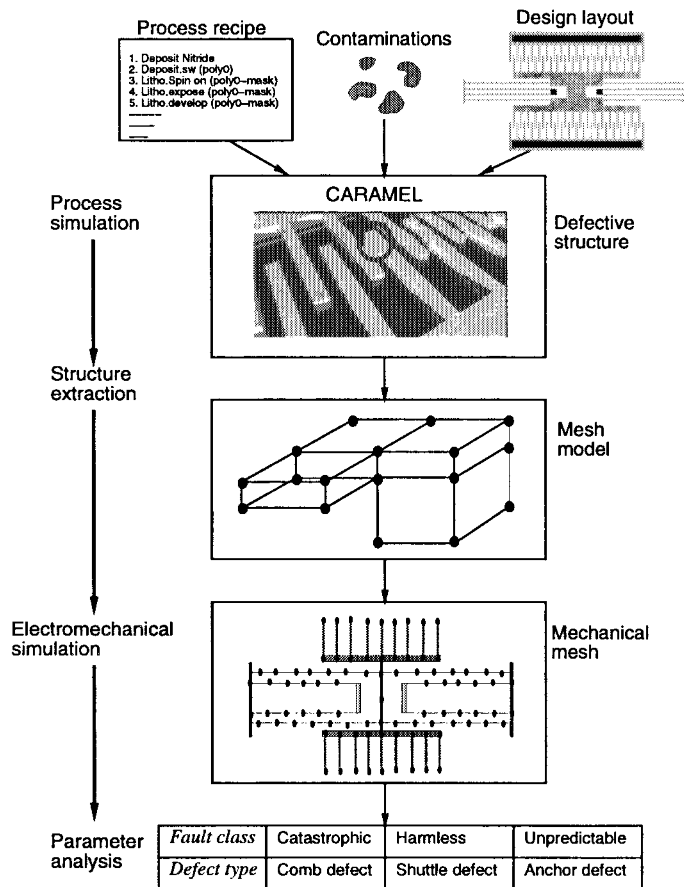

Fig. 1. MEMS particulate contamination analysis using CARAMEL.

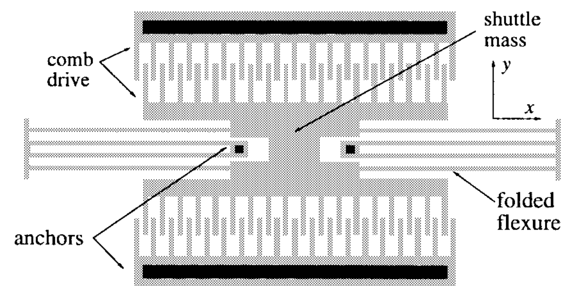

Fig. 2. Top view of a comb-drive microresonator.

Fig. 2) under consideration belongs to a class of MEMS known as surface-micromachined MEMS. Prototype surface micromachining processes are available from MCNC (Multi-user MEMS Processes service (MUMP's) [9]), Analog Devices' iMEMS process [10], and from Sandia National Labs [11]. We have selected the MUMP's process for the contaminations simulations of the resonator due to its open availability. The seminal paper on the resonator is given in [12]. Analytic models of the resonator's pertinent characteristics can be found in [13]–[15]. The resonator structure is a mature case study in the design of "suspended MEMS" which are now used in commercial accelerometers [10], [16], gyroscopes and micromirror optical beam steering [17]. Future commercial applications are in resonator-based oscillators [18], IF mixers, high-Q IF filters for communications and microstages for probe-based data storage [19].

The rest of this paper is organized as follows. Section II describes prior work in the area of MEMS testing. Section III describes MEMS contamination analysis using our tool CARAMEL. In Section IV, simulation results obtained using CARAMEL on the surface-micromachined microresonator are presented. Finally in Section V, we present conclusions.

II. Related Work

Most research in MEMS centers on design, technology, and packaging problems and not testing. However, a growing number of researchers have been concerned with MEMS testability. Here, we discuss representative work performed in this area.

Fault Modeling and Simulation of MEMS

Fault models abstract the behavior of physical defects to a high-level representation of the unit under test. In the case of MEMS, where physical failure mechanisms are much more complex due to presence of mixed domains, developing fault models becomes a difficult challenge.

In [21], an extensive overview of the issues and possible solutions for the problems related to MEMS fault modeling, simulation, test generation, design for testability, and built-in self test (BIST) is presented. MEMS defects are modeled using the concept of mutants and saboteurs. Mutants use analog-like faults to model nonelectrical (mechanical, optical, etc.) defects. Mutants represent defects that cause value changes in microstructure parameters. Saboteurs, on the other hand, model defects that cause components to be removed or added to the microstructure. Fault simulation is performed by modifying the fault-free schematic of the microsystem through the instantiation of mutants or saboteurs. A still-open question involves characterization and selection of the mutants and saboteurs that represent realistic MEMS defects.

In [22], the importance of the MEMS model and its relationship to defects of the MEMS structure is stressed. An electrical model is also used to represent mechanical and electrical components of MEMS. However, the model is constructed in a such way so as to allow the accurate modeling of a wide variety of MEMS defects. They have focused on the construction of a simulation model that eases fault injection in order to perform fault simulation. Experiments are performed on two microsystems: a resonant silicon beam force sensor and a miniature optoelectric transformer.

Most of the on-going research in MEMS fault modeling and simulation builds upon the approaches used in analog fault modeling and simulation. However, a large variety of physical, chemical and other effects complicate fault model generation for MEMS, making a purely analog-like approach inadequate.

Test Generation for MEMS

Test generation for MEMS is not a simple extension of digital or analog test techniques. The presence of multiple domains like mechanical, chemical, and optical complicates test generation. Also, the accuracy and effectiveness of test generation is highly subject to the accuracy of the fault models

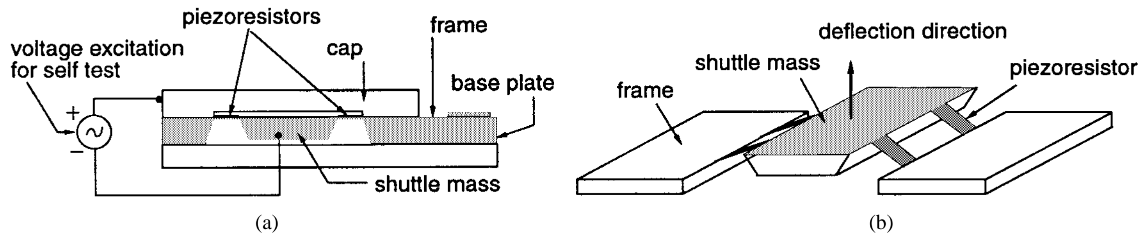

Fig. 3. Cross section of piezoresistive accelerometer die [24].

applied. Here, we discuss two approaches to the MEMS test generation problem.

The approach described in [21] is based on the sensitivity-guided search process originally described in [23]. The fault model applied uses the mutant/saboteur concept described earlier. Test generation begins with the selection of an initial test stimulus that corresponds to the mid-range of input values. A fault simulation is then performed to estimate the fault coverage. The undetected faults are resimulated using test patterns that are "higher" and "lower" than the initial input. Faults which remain undetected by the new tests are partitioned into two new lists: one containing faults for which the sensitivity of the measuring parameter has increased for higher input stimuli and another containing those faults for which the sensitivity of the measuring parameters has increased for lower input stimuli. The process is repeated until the coverage achieved is satisfactory.

Another test generation approach is presented in [20]. An electrical schematic is used to model both the electrical and mechanical components of a bulk-micromachined accelerometer. Similar to digital fault modeling, defects are modeled using stuck-at, bridging, and stuck-open faults. Carefully placed resistors are added to their electrical schematic to model these faults. Additional flexibility is provided by allowing the value of these "fault" resistors to vary. Exhaustive Hspice simulations are used to determine which voltage and current nodes are good candidates for observing faulty behavior. These simulations require sweeping the values of the fault resistors from 1 KΩ to 1 GΩ—the extremes of the value range attempts to mimic shorts and opens, respectively. Voltage and current are measured at various nodes in the circuit for every value of the fault resistor. Measurement windows for ranges of voltage and current for which a circuit is defined to be faulty or fault-free are established. Faults are selected through the analysis of real accelerometer failures. From this information, the location of the most sensitive nodes for detecting accelerometer failures are identified.

BIST and Fault Tolerance for MEMS

Next, we describe the research performed in the areas of built-in self test (BIST) and fault tolerance for MEMS. Similar to MEMS fault simulation and fault modeling, ideas presented in these areas also leverage techniques from analog test. There are two broad classes of BIST that can be identified. Spatial redundant techniques use additional circuitry to perform the self test. These include specific test/monitoring cells [26], [27], analog test buses, and circuit duplication. Analytical redundant techniques, on the other hand, use parametric analysis, frequency spectrum characteristics [28], reliability indicators [29], and signal delay measurements. Most BIST approaches for MEMS use a combination of the two approaches.

In [24], a BIST approach for a piezoresistive accelerometer is described. Fig. 3 shows a cross section of the accelerometer. During test, a self-testing voltage is stepped from +20 V to −20 V and the sensor output is measured. At every applied voltage, shuttle mass acceleration and the sensitivity (V/g) of the device is computed to verify whether the device is functional. Structural design modifications are suggested for protecting the device from excessive force. The self-testing feature provides two benefits. The first is that the user can confirm that the shuttle-mass is unrestricted and therefore free to respond in critical operating conditions. Secondly, the self-test applies a known electrostatic force to the mass which cannot be differentiated from an acceleration force. Hence, the self-test can be used for calibration.

Built-in self test approaches for micromachined accelerometers described in [24] and [30] rely on the application of electrostatic forces to the silicon mass. The electrostatic forces are fundamentally weak thus making the use of very high voltages necessary to achieve full-scale electrostatic actuation in accelerometers. This is the main drawback in using electrostatic actuation for implementing built-in self test for MEMS-based devices.

In [31], a thermal self-test mechanism is proposed to overcome this drawback for accelerometers with a 50-G full-scale deflection. This technique uses a differential thermal expansion to provide actuation. The BIST structure used is virtually insensitive to ambient temperature variations and thus has no effect on the thermal performance of the sensor. Fig. 4 shows an illustration of an accelerometer with thermal self test. The self-test feature uses an actuation beam that is thermally isolated from the seismic mass (suspended silicon) by a gap of 8 μm. An ion-implanted heating resistor is located near the middle of the central beam. When a voltage pulse is applied to the heat resistor, the temperature of the actuation beam increases. The temperature change causes the beam to expand which creates a force on the mass that causes a downward movement. The piezoresistive sense elements detects the downward motion of the mass as an acceleration signal.

Summary

We have presented an overview of the research in MEMS testing. Others have also contributed to the area [27], [33]–[35]. In the following, we list our general observations.

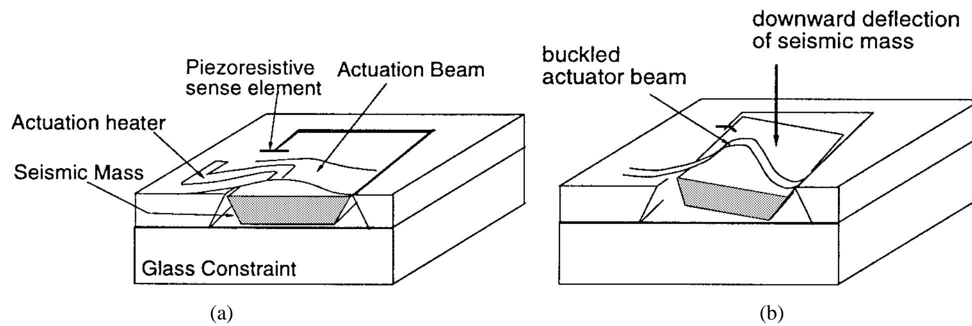

Fig. 4. An accelerometer with thermal self test [31].

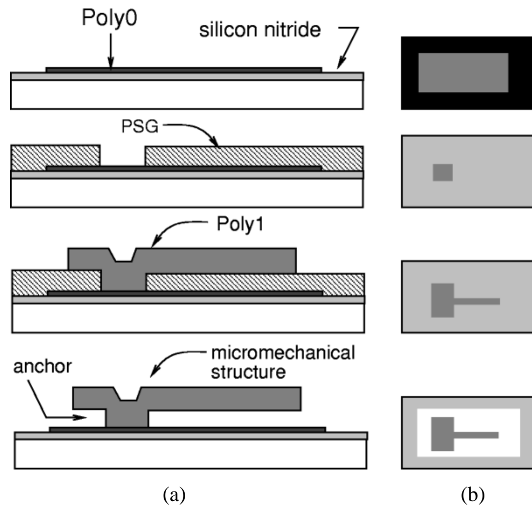

Fig. 5. Abbreviated flow for MCNC's MultiUser MEMS Process service [9]. (a) Cross-sectional view. (b) Top view (layout).

1) The MEMS testing techniques described in the literature are highly design specific. As a result, they may be inapplicable to other designs. Hence, there is a need to develop a testing methodology which is applicable to all instances of a class of MEMS structures. The long-term objective of our research work is to develop such a testing methodology for surface-micromachined MEMS.
2) The success of any testing technique depends on the fault models applied. The fault models described in the literature are also design specific and are in general difficult to apply. We plan to address this problem by developing realistic fault models that can be applied to a class of MEMS designs at a higher level of abstraction.
3) Most BIST techniques estimate the mechanical movement of the microstructure by performing electrical measurements. Measurements of small mechanical movements are difficult, if not impossible, to perform because of the presence of noise. Thus, most measurements occur at or near full scale. Setting the range for fault-free behavior, as in analog testing, is a difficult task and constraints that limit the thresholds used may result in information loss that degrades test quality. This problem can be handled by analyzing all the possible failure mechanisms and the resulting deviations in the final functionality. Knowledge of such correlations will lead to more effective BIST techniques (like modification of structural and material properties, selection of better measurement techniques), and aid in MEMS fault diagnosis. Therefore, our work in MEMS testing first centers on exploring defects caused by particles and the associated misbehaviors.

III. CARAMEL

CARAMEL is a process simulator that maps particle contaminations to defective microstructures. It is built around the tool CODEF, which is a contamination-to-defect-to-fault mapper for pure electrical layouts [1]. Described next are the three phases of CARAMEL's operation.

A. Process Simulation

This phase of CARAMEL maps spot contaminations to layout defects and is implemented using a modified version of CODEF. CODEF determines the impact of a particle on the contaminated region of an IC layout. It accepts layout information, a process description, and contamination statistics for each processing step of interest. CODEF allows for the exact characteristics of the contamination particle to be simulated including the particle's size, density, conductivity, and fabrication step of introduction. Given the contamination parameters, it simulates all the fabrication steps and creates a three-dimensional (3-D) representation of the defective device. CODEF, in its unmodified form, is used to analyze the effects of particles on an electrical IC layout. It utilizes a circuit extractor which traverses the 3-D structure to create a SPICE netlist. Defective circuit behavior resulting from the contaminations can then be analyzed through SPICE simulations.

To make use of CODEF for MEMS contamination analysis, we have defined a complete MUMP's fabrication process as a sequence of steps in the PREDITOR format [36]. The MUMP's process is used to form micromechanical structures composed of thin films formed on the surface of the substrate. These thin-film microstructures are called surface-micromachined MEMS. Because the resonator is a single-polysilicon structure, fabrication of the resonator utilizes only a subset of the complete three-polysilicon MUMP's process. This simplified version of the MUMP's process is described in [37] and is illustrated in Fig. 5. First, a low-stress silicon nitride is deposited on the silicon substrate to provide electrical isolation between microstructures. An electrical interconnec-

tion layer of polysilicon is then deposited and patterned. Next, a 2-μm-thick layer of phosphosilicate glass (PSG) is deposited. PSG acts as sacrificial spacer layer for the microstructures. After contact cuts are made in PSG, a 2-μm-thick layer of polysilicon is deposited and patterned to form a microstructure. A final wet etch in hydrofluoric acid (HF) dissolves the PSG and releases the microstructure so that it is free to move. Contact cuts in the PSG are anchor points that fix the microstructure to the substrate.

In CARAMEL, we have modified CODEF to handle the MUMP's "release" step (i.e., the HF etch of PSG) as described above. Adding this step, which is not part of any standard CMOS process, allows us to perform MUMP's process simulations using realistic contaminations.

B. Structure Extraction

The structure extraction phase produces a 3-D mesh representation of the defective structure generated by CODEF. Mechanical simulation of the mesh (using finite-element analysis (FEA) tools like ABAQUS [8]) allows detailed analysis of the effects of contaminations on the mechanical structure.

The process simulator creates a 3-D representation of the resonator structure consisting of hierarchically connected layers of material known as the Chip Data Base (CDB) [39]. CDB is created from the MUMPS process flow and the CIF layout of the resonator. In addition, contamination particles may be introduced at random locations in the process flow, under control of the process simulator, which can alter the final 3-D structure of the resonator structure. CARAMEL creates a separate "mesh database" from the CDB to represent the MEMS structure as a set of two-dimensional (2-D) corner-stitched rectangular regions [40]. Each region of the mesh consists of a set of material elements. However, the mesh database differs from a traditional corner-stitched database because elements in the former are allowed to be less than maximal width. This is a necessary feature since the mesh used for mechanical simulation requires that each region have a single neighbor or no neighbor along each of its edges. Each element also has associated data that describes its material characteristics, its position in the z direction, and a flag that indicates if the base of the element is anchored.

The MEMS meshing phase accomplishes the following.

1) Creates a corner-stitched database containing the regions to be simulated.
2) Determines the connectivity of the regions.
3) "Splits" the mesh database to ensure that each region has only one or zero neighbors in the x, y, and z directions.
4) Identifies the elements and generates node numbers for all the vertices of every region. (This is required by the FEA tool for mechanical simulation.)
5) Generates the final mesh input model for the FEA tool.

Mesh Database Creation: The mesh database for the resonator consists only of polysilicon one (POLY1) and defect material, i.e., the material of the particle contamination. The mesh is created by examining every region of CODEF's CDB. Each element of POLY1 or defect material is added to the mesh database along with a flag indicating if the element is fixed to some other material or contains free space underneath. The flag information is used later to determine which elements are free to move.

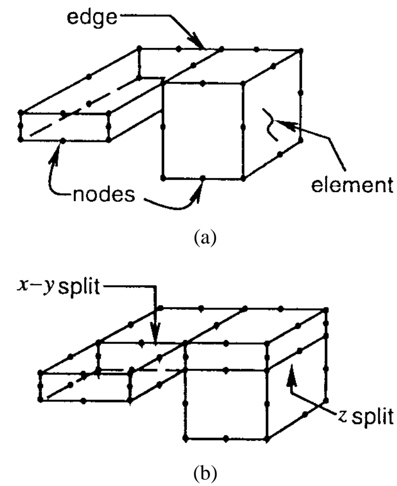

Fig. 6. Illustration of element splitting for mechanical mesh construction. (a) Set of regions before split. (b) The same regions after x-y and z splits.

Determining Element Connectivity: Understanding the behavior of the resonator requires mechanical simulation of its moving parts. The moving parts of the resonator includes the shuttle mass and everything connected to the shuttle. Because a particle contamination can alter the topography of the resonator, the resulting defective structure must be derived from the CDB of elements. In this phase, CARAMEL determines all the connected elements from a user-specified element on the resonator's layout. A simple algorithm is employed that marks the user-specified element and continues to mark neighboring elements until all connected regions are marked.

Element Splitting: The mechanical mesh required by FEA tools must be constructed so that adjacent regions meet only at region vertices (nodes). CARAMEL must meet this adjacency constraint not only in the x and y directions but also in the z-direction.

- x-y **splitting:** In a standard corner-stitched database, a region edge can have multiple neighboring regions or a partial neighbor as shown in Fig. 6(a). Such a situation violates the constraint described above for the mechanical mesh. The x-y splitting operation modifies an element so that every region edge has a single neighboring element or no neighbor at all. Splitting is performed by analyzing the edge neighbors of every region in the CDB. For each edge that violates the constraint, the current region is split at the neighbor's edge. (See Fig. 6.)
- z **splitting:** In an analogous way, elements may need to be split in the z direction as well. In this case, adjacent regions that have elements of differing heights must be split in the z direction so that the resulting elements share nodes. This is accomplished using a simple algorithm that compares the top and bottom coordinates of an element with all its neighboring elements. If an adjacent element is contained in the current element, the current element is split. (See Fig. 6.) There is one exception

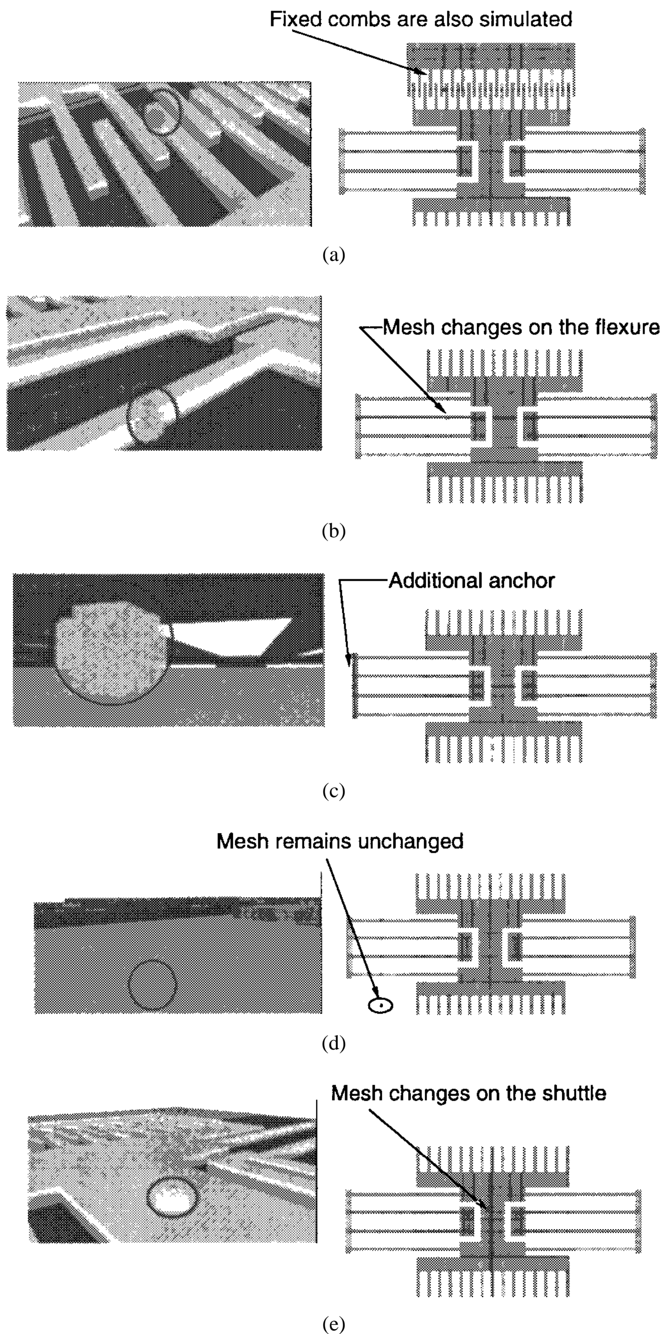

Fig. 7. Three-dimensional representations of defective resonators and their corresponding mechanical mesh for a particle contamination located (a) between adjacent comb fingers, (b) in a beam, (c) under the flexure, (d) outside of the resonator's active area, and (e) on the shuttle.

to the z-split operation when the element of concern is fixed. Typically, split elements inherit identical properties (material, conductivity, etc.) from the original element. In the case of fixed elements, only the newly created bottom-half element is fixed.

The result of CARAMEL's extraction phase is a mechanical mesh that is directly compatible with the FEA tool ABAQUS. The resulting mechanical mesh captures the impact of the particle contamination on both the electrical and mechanical properties of the resonator. It should be noted here that CARAMEL is a general tool and is therefore not restricted to the resonator but is applicable to any generic MEMS layout. It is therefore possible to analyze the impact of particle contaminations on a wide variety of MEMS topologies. In the next section, we examine the impact of 4000 contaminations on the structure and behavior of the resonator.

IV. Simulation Results

CARAMEL was used to analyze 4000 unique contaminations of the resonator. We analyzed contaminations of various sizes and material properties. In addition, contaminations were placed at many different resonator locations and were introduced randomly across all the steps of the MUMP's process. The effect of each particulate was observed at each phase of CARAMEL's operation. The mechanical simulator ABAQUS was also used to compute the maximum displacement of the movable shuttle for each of the mechanical meshes generated by CARAMEL. Displacement is analyzed because it is one of the crucial parameters for determining if the resonator is functioning properly; analysis of any other parameter can also easily be done. In Table I, details of several representative cases of the contamination analysis are presented. Note that the first entry of Table I gives the maximum displacement for the defect-free resonator. For each case considered, the location of the contamination (Table I), the resulting 3-D defective structure (Figs. 7 and 8), and the resulting maximum displacement as reported by ABAQUS (Table I) are given.

- **Comb Defect:** Fig. 7(a) shows the impact of a contamination located between adjacent comb fingers. The process simulation phase of CARAMEL reveals that the contamination welds together the two normally moving fingers. The fixed fingers transforms the two comb drives into a single structure thereby changing the mesh model required for mechanical simulation. Mechanical simulation of a defect-free resonator requires only the shuttle and flexure. The result obtained from FEA reveals shuttle movement is impossible—a clear indication that this defect has caused a catastrophic failure.
- **Beam Defect:** The impact of a defect affecting a beam of the folded-flexure is illustrated in Fig. 7(b). Such a contamination results in a slightly heavier beam. The increased mass of the beam has a negligible effect on the y displacement. Note the complexity of the mesh in the area surrounding the defect's location. The increased "meshing" is a reflection of the number of splits required to accurately represent the region containing the defect.
- **Flexure Defect:** A contamination that becomes lodged between the resonator and the substrate acts as an anchor. CARAMEL handles such cases by defining an anchor element at the contamination location during the extraction phase. The meshing phase discovers that the contaminant is connected to the suspended structure and the substrate surface. The resulting mesh used in the mechanical simulation therefore has an extra anchor. The impact of such a defect is shown in Fig. 7(c). Simulation of the corresponding mesh indicates that the deflection has slightly reduced to the value of 3.21 nm, a deviation of 2%. Other simulations show that the displacement

TABLE I
REPRESENTATIVE CASES OF DEFECT ANALYSIS USING CARAMEL

Particle location	Diameter size (μm)	Density (kg/m^3)	Added after step	Displacement in y (nm)	Percentage change in y displacement (%)
None	-	-	-	3.26	-
Comb	2.4	2330	Poly1 deposition	0	-100
Beam	1.5	2330	PSG deposition	3.26	0
Flexure	2.0	2330	Poly0 PR Strip	3.21	-2
Outside	2.0	2330	Poly0 deposition	3.26	0
Shuttle	1.5	2330	PSG deposition	3.25	≈0
Broken beam	1.5	2330	Poly1 PR deposition	4.06	+25

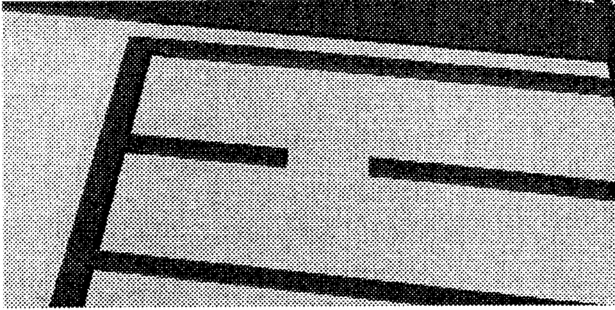

Fig. 8. Broken spring beam resulting from a particle introduced before the photoresist deposition for the structural layer.

reduction is greater as the anchor location moves closer to the shuttle, an intuitive result since the resonator becomes stiffer with anchor movement toward the shuttle.

- **Outside Defect:** Contaminations lying outside the structure are treated like the others, but during the connectivity phase of meshing, it is determined that the contaminant is not connected to the structure of interest. Meshes for such defects are generated but are not simulated. For these cases the nominal values of resonant frequency are reported. An example of this type of defect is illustrated in Fig. 7(d).
- **Shuttle Defect:** Fig. 7(e) shows another interesting case where the contamination becomes totally encapsulated by the shuttle mass. Process simulation indicates that a small bump is formed on the shuttle surface. The creation of such a bump changes the meshing of the affected region which is apparent from the dense meshing surrounding the defect location. FEA reveals a very small decrease in displacement due to the additional mass.
- **Broken Beam:** Broken structures can also result from the presence of particles. Fig. 8 shows a broken spring beam caused by a particle introduced before the photoresist deposition for the structural layer. Presence of the particle during this step creates a vulnerable location in the structural material at the location of the particle. The overetching that takes place at this location creates a broken structure. FEA of this defective structure results in a 25% increase in deflection, an intuitive result since the flexure spring is now floppier.

The analyzed cases demonstrate CARAMEL's ability to model and simulate a variety of contamination effects on the MEMS microstructure. The tool can be effectively used to generate several thousand contamination simulations under a Monte-Carlo mode of operation. In Monte Carlo mode, contaminations are introduced into the process at random steps, with random sizes and at random locations in the layout. Such an analysis can produce the full spectrum of MEMS failure modes due to particulates. The observed deviations in behavior can then be systematically categorized under various fault classes. These fault classes can then be mapped to appropriate fault models at the higher level of abstraction. In other words, such an analysis provides a technique for abstracting defective beams, gaps, shuttles, etc. into higher level fault models. We have performed 4000 simulations using CARAMEL to illustrate its Monte-Carlo mode of operation. Process simulation showed that only 492 contaminants resulted in defective microstructures. The remaining contaminations either did not come into contact with the structure or were naturally removed by the process.

Table II presents a coarse fault categorization of the 492 defects. The three broad fault classes are identified as catastrophic, parametric, and harmless. Catastrophic defects are those defects that cause more than a 30% change in the maximum achievable displacement in the y direction. Defects that cause a displacement deviation between 5% and 30% are termed parametric. Defects are classified as harmless and within the specification if they have a negligible affect (<5%) on displacement.

Table III shows the occurrences of defects with respect to the process step of introduction. This information identifies the MUMP's process steps that are most vulnerable to particle contaminations. It is obvious that step 8 (the etch of the resist for Poly0, the first layer of polysilicon) is highly prone to catastrophic failures. This result is quite intuitive. Poly0 forms the base of the resonator while the suspended structure is formed from Poly1, the second layer of polysilicon. Hence, any contamination occurring on Poly0 can bind the two layers and impede resonator movement. This situation often leads to catastrophic failures. Thus, the Poly0 deposition and development phases of fabrication are quite vulnerable to particle contaminations. As indicated in Table III, contaminations introduced during this phase (steps 1–3 and 8) lead to over 60% of the catastrophic failures observed.

Table IV shows the spatial distribution of the contaminations over the resonator layout that caused catastrophic and parametric failures. This categorization of the defects shows that the shuttle is the most defect-prone region in the resonator

TABLE II
COARSE FAULT CATEGORIZATION BASED ON DEVIATION FROM THE NOMINAL y DISPLACEMENT

Defect type	Number of occurrences	Deviation in y	Comments
Catastrophic	223	$\Delta y > 30\%$	Resonator movement is outside specification.
Parametric	16	$5\% \leq \Delta y \leq 30\%$	Resonator still operates but with large deviations from the desired displacement.
Harmless	253	$\Delta y < 5\%$	Resonator displacement within specifications.

TABLE III
DEFECT CATEGORIZATION BASED ON THE MUMPS PROCESS STEP FOR WHICH THE CONTAMINATION WAS INTRODUCED

Process step	No. of occurrences	No. of catastrophic faults	No. of parametric faults	No. of harmless faults
1 (Initialize)	43	40	3	0
2 (Nitride deposit)	42	38	2	1
3 (Poly0 deposit)	50	48	3	2
8 (Etch Poly0 resist)	42	39	2	0
15 (Poly1 deposit)	28	0	3	25
16 (Litho spinon Poly1)	36	4	0	28
17 (Litho expose Poly1)	34	7	0	30
18 (Litho develop Poly1)	31	4	0	27
20 (Etch Poly1 resist)	71	3	0	68
21 (PSG release)	115	40	3	72
Total defects	492	223	16	253

TABLE IV
SPATIAL DISTRIBUTION OF FAULTS IN THE MICRORESONATOR

Particle location	Catastrophic faults (%)	Parametric faults (%)	Total (%)
Shuttle	69.2	6.25	61.3
Comb fingers	21.6	6.25	22.0
Folded flexure	9.2	87.5	16.7

encompassing approximately 70% of the total number of catastrophic faults. Defects affecting the comb fingers have resulted in significant changes in behavior. However, the shuttle, due to its relatively large area is likely to be "hit" by a contamination, thus making this region of the resonator highly susceptible to failure in the presence of a randomly introduced particle. The smaller surface area of the folded-flexure beams, on the other hand, is less likely to be affected. But when these beams are impacted, their behavior is significantly altered.

It is also important to note that all the catastrophic failures due to shuttle contaminations occur before deposition of the Poly1 layer. These contaminations create anchors between the Poly1 and Poly0 layers. Conversely, contaminations occurring on the shuttle after/during Poly1 deposition do not cause appreciable change in shuttle displacement. Thus, the impact of particle contaminations on resonator behavior is a function of both the location and the process step of introduction.

The following are the main observations that can be drawn from the simulation results.

1) Particle contaminations can have a large impact on the resonator functionality and the resulting spectrum of faulty behaviors can be discovered through contamination and FEA simulations.
2) A systematic classification of the faulty behavior can be made by mapping various fault classifications to a higher level of abstraction.
3) Impact of particle contamination is a function of both the location and process step in which it is introduced.
4) The comb drive is the most defect prone region of the resonator and particle contaminations that occur during the Poly0 deposition process steps are the most likely to cause a failure.

V. CONCLUSIONS

We have automated the contamination analysis process for microelectromechanical layout using our tool CARAMEL. CARAMEL can be effectively used to directly investigate the faulty behavior of defective MEMS structures. Here, we have illustrated CARAMEL's use on a folded-flexure resonator. Analysis of 4000 different particle contaminations indicates that spot contaminations can have a significant impact on the maximum displacement of the resonator. Moreover, the results show that the impact of a particular defect is highly dependent upon where it is located in the resonator's layout and when it is introduced into the manufacturing process. Particulates that create anchor defects near or on the shuttle or weld

comb fingers cause catastrophic failures. Anchor defects away from the shuttle affecting the folded flexure cause parametric changes in behavior.

CARAMEL is being used to formulate fault models for MEMS primitives, (i.e., beams, anchors, springs, suspended masses, etc.) the basic elements used in resonator, accelerometer, and gyroscope designs. The objective here is to abstract the misbehaviors (all changes in specified behavior) due to particulates into a high-level simulator such as NODAS [41]. Meeting such an objective will enable the evaluation and optimization of the testability of a large class of MEMS. Specifically, accurate fault models will enable:

- **Test Methodology Grading:** Given an accurate fault model, one can measure the effectiveness of any given test methodology. Presumably, the fault model will provide an enumeration of possible faulty behaviors along with their likelihood of occurrence. Coverage figures for current MEMS testing methods can then be determined through systematic fault simulations.
- **Test Methodology Development:** Any possible shortcomings in current testing methodologies will be exposed by test methodology grading. Even if shortcomings do not exist, knowledge about MEMS faulty behavior may lead to more effective test or design techniques that reduce cost and/or increase quality.
- **MEMS Diagnosis:** More effective testing methodologies will undoubtedly lead to better diagnosis. We plan to create links between observed faulty behavior, testing methods, and failure sources for accurate and efficient improvements in diagnostic techniques.

Our future work will also include the formation of fault models for other failure sources such as stiction, undesired residual stress, and extreme manufacturing variations.

REFERENCES

[1] J. Khare and W. Maly, *From Contamination to Defects, Faults and Yield Loss.* Boston, MA: Kluwer, 1996.

[2] R. D. Blanton, G. K. Fedder, and T. Mukherjee, "Hierarchical design and test of MEMS," *Microsystem Technology News*, Apr. 1998, pp. 28–31.

[3] G. K. Fedder, S. Iyer, and T. Mukherjee, "Automated optimal synthesis of microresonators," in *Tech. Dig. IEEE Int. Conf. Solid State Sensors and Actuators*, vol. 2, June 1997, pp. 1109–1112.

[4] T. Mukherjee and G. K. Fedder, "Structured design of microelectromechanical systems," in *Design Automation Conf.*, June 1997, pp. 687–685.

[5] A. Kolpekwar, R. D. Blanton, and D. Woodilla, "Failure modes for stiction in surface-micromachined MEMS," in *Int. Test Conf.*, Oct. 1998.

[6] A. Kolpekwar and R. D. Blanton, "Development of a MEMS testing methodology," in *Int. Test Conf.*, Nov. 1997, pp. 923–931.

[7] J. Khare, W. Maly, and N. Tiday, "Fault characterization of standard cell libraries using inductive contamination analysis (ICA)," in *VLSI Test Symp.*, Apr. 1997, pp. 405–413.

[8] *ABAQUS User Manual*, vol. 2, Hibbit, Karlsson & Sorensen, Inc., Pawtucket, RI, 1995.

[9] D. A. Koester, R. Mahadevan, and K. W. Markus, "Multi-user MEMS processes (MUMPS): Introduction and design rules." Available: mems.mcnc.org/mumps.html, Oct. 1994.

[10] "ADXL series accelerometer datasheets." Available: www.analog.com, Analog Devices Inc., Norwood, MA, 1996.

[11] "Intelligent MicroMachine Initiative." Available: www.mdl.sandia.gov /Micromachine, Sandia National Laboratories, Livermore, CA.

[12] W. C. Tang, T. C. H. Nguyen, M. W. Judy, and R. T. Howe, "Electrostatic comb drive of lateral polysilicon resonators," *Sens. Actuators A*, vol. 21, nos. 1–3, pp. 328–331, Feb. 1990.

[13] G. K. Fedder, "Simulation of microelectromechanical systems," Ph.D. dissertation, Univ. Calif. at Berkeley, Sept. 1994.

[14] Z. Zhang and W. C. Tang, "Viscous air damping in laterally driven microresonators," in *IEEE Micro Electro Mechanical Systems Workshop*, Jan. 1994, pp. 199–204.

[15] W. A. Johnson and L. K. Warne, "Electrophysics of micromechanical comb acutators," *IEEE J. Microelectromech. Syst.*, vol. 4, pp. 49–59, Mar. 1995.

[16] "MMAS40G10D Accelerometer Datasheet," Available: www. motorola.com. Motorola, Semiconductor Products Sector, Austin, TX, 1996.

[17] M. A. Mignardi, "Digital micromirror array for projection TV," *Solid State Technology*, vol. 37, no. 7, pp. 63–64, July 1994.

[18] C. T. C. Nguyen and R. T. Howe, "CMOS micromechanical resonator oscillator," in *IEEE Int. Electron Devices Meeting*, 1993, pp. 199–202.

[19] G. K. Fedder *et al.*, "Laminated high-aspect-ratio microstructures in a conventional CMOS process," in *IEEE Micro Electro Mechanical Systems Workshop*, Feb. 1996, pp. 13–18.

[20] T. Olbrich, A. Richardson, W. Vermeiren, and B. Straube, "Integrating testability into microsystems," *Microsystem Technologies*, Feb. 1997, pp. 72–79.

[21] M. Lubaszewski, E. F. Cota, and B. Courtois, "Microsystem testing: An approach and open problems," *Design and Test in Europe*, Feb. 1998.

[22] W. Vermeiren, B. Straube, and A. Holubek, "Defect-oriented experiments in fault modeling and fault simulation of microsystem components," in *European Design and Test Conf.*, Mar. 1996.

[23] N. Nagi, A. Chatterjee, A. Balidava. and J. A. Abraham, "Fault based automatic test generator for linear analog circuits," in *IEEE/ACM Int. Computer-Aided Design Conf.*, Nov. 1993.

[24] H. V. Allen, S. C. Terry, and D. W. DeBruin, "Accelerometer systems with self-testable features," *Sensors and Actuators A*, 1989, pp. 153–161.

[25] L. Zimmermann, "Airbag application: A microsystem including a silicon capacitive accelerometer, CMOS switched-capacitor electronics and true self-test capability," *Sensors and Actuators A*, 1995, pp. 190–195.

[26] R. Harjani and B. Vinnakota, "Analog circuit observer blocks," *IEEE Trans. Circuits and Systems II*, vol. 44, no. 3, pp. 154–163, 1997.

[27] T. Olbrich, D. A. Bradley, and A. Richardson, "Built-in self test and diagnostic for microsystems," in *Int. Symp. Advanced Transport Applications*, 1994, pp. 511–519.

[28] K. Arabi, B. Kaminska, and J. Rzeszut, "BIST for D/A and A/D converters," *IEEE Design Test Comput.*, vol. 13, no. 4, pp. 40–49, 1996.

[29] T. Olbrich, A. Richardson, and D. A. Bradley, "BIST & diagnostics in safety critical microsystems using reliability indicators," in *European Symp. Reliability of Electronic Devices Failure Physics and Analysis*, Oct. 1994, pp. 4–7.

[30] T. Core, R. S. Payne, D. Quinn, S. Sherman, and W. K. Wong, "Integrated complete, affordable accelerometer for air-bag applications," in *Sensors Exposition*, 1991, pp. 204–210.

[31] F. Purahmadi, L. Christel, and K. Petersen, "Silicon accelerometer with new thermal self-test mechanism," in *IEEE Solid-State Sensor and Actuator*, June 1992.

[32] P. Ohlckers *et al.*, "An integrated resonant accelerometer microsystem for automotive applications," in *Int. Conf. Solid-State Sensors and Actuators*, June 1997.

[33] T. Olbrich, D. Bradley, and A. Richardson, "Self-test and diagnostics for smart sensors in automotive applications," in *IEE Colloquium on Automotive Sensors*, Sept. 1994.

[34] W. Vermeiren, B. Straube, and G. Elst, "Microsystem fault simulation-aspects and requirements," *Micro System*, Oct. 1994.

[35] C. Kantzsch *et al.*, "Micro system design for testability," *Microsystem Technologies*, 1991.

[36] D. M. H. Walker, C. S. Kellen, and A. J. Strojwas, "The PREDITOR process editor and statistical simulator," in *Int. Workshop on VLSI Process and Device Modeling*, May 1991, pp. 120–123.

[37] G. K. Fedder and T. Mukherjee, "Physical design for surface-micromachined MEMS," *ACM/SIGDA Physical Design Workshop*, Apr. 1996, pp. 53–60.

[38] A. Kolpekwar, C. Kellen, and R. D. Blanton, "Fault model generation for MEMS," in *Int. Conf. Modeling and Simulation of Microsystems, Semiconductors, Sensors and Actuators*, Apr. 1998, pp. 111–116.

[39] D. M. H. Walker, C. S. Kellen, D. M. Svoboda, and A. J. Strojwas, "The CDB/HCDB semiconductor wafer representation server," *IEEE Trans. Computer-Aided Design*, vol. 12, pp. 283–295, Feb. 1993.

[40] J. K. Ousterhout, "Corner stitching: A data-structuring technique for VLSI," *IEEE Trans. Computer-Aided Design*, vol. 3, pp. 87–100, Jan. 1984.

[41] J. E. Vandemeer, M. S. Kranz, and G. K. Fedder, "Hiearchical representation and simulation of micromachined inertial sensors," in *Int. Conf. Modeling and Simulation of Microsystems, Semiconductors, Sensors and Actuators*, Apr. 1998.

Abhiject Kolpekwar received B.E. degree in electrical and electronic engineering and M.S. degree in physics from Birla Institute of Technology and Science, Pilani, India, in 1995. He received the M.S. degree in computer engineering in 1998 from Carnegie Mellon University, Pittsburgh, PA.

He is currently working as Senior Member of Technical Staff of Cadence Design Systems. His research was mainly focused in the area of MEMS Testing.

Tao Jiang received the B.S. and M.S. degrees in electrical engineering from Tsinghua University, China, in 1995 and 1997, respectively. He is currently a graduate student in the Center for Electronic Design Automation at Carnegie Mellon University where he has been working on the development of a general test methodology for surface-micromachined MEMS since 1998. His current research mainly focuses on MEMS failure analysis and fault modeling.

R. D. (Shawn) Blanton (M'93) received the Bachelor's degree in engineering from Calvin College, Grand Rapids, MI, in 1987, the Master's degree in electrical engineering from the University of Arizona, Tucson, in 1989, and the Ph.D. degree in computer science and engineering from the University of Michigan, Ann Arbor, in 1995.

He is currently an Assistant Professor in the Department of Electrical and Computer Engineering, Carnegie Mellon University, where he is a member of the Center for Electronic Design Automation. His research interests include the computer-aided design of VLSI circuits and systems, fault-tolerant computing and diagnosis, verification and testing, and computer architecture. He has worked on the design and test of complex systems with General Motors Research Laboratories, AT&T Bell Laboratories, Intel, and Motorola.

Dr. Blanton is the recipient of a National Science Foundation Career Award and is a member of ACM.